Journal of Solid State Chemistry **148,** 93–99 (1999)
Article ID jssc.1999.8377, available online at http://www.idealibrary.com on IDEAL®

Modulated Structure of $La_{1/3-x}Li_{3x}NbO_3$ $0 \leq x \leq 0.06$ Perovskite-Related Materials

S. García-Martín and M. Á. Alario-Franco

Departamento de Química Inorgánica, Facultad de C.C. Químicas, Universidad Complutense de Madrid, Madrid-28040, Spain

Received February 5, 1999; in revised form April 23, 1999; accepted May 10, 1999

DEDICATED TO C. N. R. RAO IN HIS 65TH BIRTHDAY

The microstructure of samples of different composition belonging to the cation-deficient $La_{1/3-x}Li_{3x}NbO_3$, $0 \leq x \leq 0.06$, solid solution has been studied by selected area electron diffraction and high resolution transmission electron microscopy. The materials show a perovskite-related structure with basic lattice parameters $a \sim \sqrt{2}a_p$, $b \sim \sqrt{2}a_p$, $c \sim 2a_p$. Besides, short-range cation ordering gives place to a larger unit cell of dimensions $a \sim 3.5\sqrt{2}a_p$, $b \sim \sqrt{2}a_p$, $c \sim 4a_p$. The lithium-containing compunds also present a complex microdomain structure of the octahedra tilting framework. © 1999 Academic Press

***Key Words*: perovskite; lithium conductors; niobates; modulated structure; microdomains.**

1. INTRODUCTION

Research on lithium ion-conducting perovskites has achieved a great importance due to their potential applications as solid electrolytes for solid state lithium secondary batteries. Much of the work has been focused on the ionic conductivity and crystal structure of the compounds of general formula $RE_{2/3-x}Li_{3x}TiO_3$ (*RE*, rare earth ion) (1–13). These materials have a perovskite-related structure (ABO_3) with A-cation deficiency which seems to be favourable for the high Li^+ ion conductivity observed.

The perovskite structure tolerates total or partial substitution of the A and B cations by ions in different valence states, which can affect the structure and physical and chemical properties of the obtained materials. In this sense, the composition range, crystal chemistry, and ionic conductivity of the new cation deficient $La_{1/3-x}Li_{3x}NbO_3$ solid solution has recently been reported (14, 15). The range of existence of the solid solution appears to be $0 \leq x \leq 0.06$ and σ values of the order $3\text{–}4 \times 10^{-5}\,\Omega^1\,cm^{-1}$ at room termperature are found (14).

The $RE_{1/3}NbO_3$ compounds with perovskite-related structure were first described by Iyer and Smith (16) and later by Trunov *et al.* (17). The rare earth ions and vacancies are ordered within alternate (001) planes doubling the *c*-parameter of the cubic perovskite-type cell and leading to a slightly distorted orthorhombic lattice with parameters $a \sim a_p$, $b \sim b_p$, $c \sim 2a_p$ (p refers to the perovskite unit cell). Studies on $La_{1/3}NbO_3$ single crystals by Labeau (18) indicate a basic diagonal unit cell, $a \sim \sqrt{2}a_p$, $b \sim \sqrt{2}a_p$, $c \sim 2a_p$, and reveal an additional short-range La-cation ordering. Moreover, a cubic $La_{1/3}NbO_3$ has been quenched from high temperature (19) and α-$Ln_{1/3}NbO_3$ with monoclinic symmetry has been prepared under hydrothermal conditions (20).

Transmission electron microscopy has proved to be a powerful, almost inevitable tool to study the A-cation ordering in A-deficient perovskites. The structure determined by powder X-ray diffraction is usually an average structure while electron microscopy can provide complementary information on local arrangements. We present here a microstructural characterisation of the $La_{1/3-x}Li_{3x}NbO_3$ ($0 \leq x \leq 0.06$) solid solution studied by selected area electron diffraction (SAED) and high resolution transmission electron microscopy (HRTEM).

2. EXPERIMENTAL

Different compositions of the $La_{1/3-x}Li_{3x}NbO_3$ ($0 \leq x \leq 0.06$) solid solution were prepared, as described in Ref. (14), from stoichiometric amounts of Li_2CO_3, La_2O_3, and Nb_2O_5. The mixtures were heated at 700°C for several hours for decarbonation. After grinding, the samples were pelleted, covered with powder of the same composition to prevent lithia loss, and fired at 1100°C for 12 h followed by further grinding, repelleting, and refiring at 1200°C for another 12 h. Samples were removed from the furnace at 1200°C.

Crystalline phase identification was carried out by powder X-ray diffraction using a Philips X'PERT diffractometer with Cu$K\alpha_1$ radiation, a curved Cu monochromator, and PEAPD (Philips) software. The molar ratio of the metals in

0022-4596/99 $30.00

the compounds was determined by inductive coupled plasma (ICP) spectroscopy using a JY-70 Plus instrument. Results are shown in Ref. (14).

For transmission electron microscopy, the samples were ground in *n*-butyl alcohol and ultrasonically dispersed. A few drops of the resulting suspension were deposited in a carbon-coated grid. SAED studies were performed with an electron microscope JEOL 2000FX (double tilt $\pm 45^\circ$) working at 200 KV and HRTEM studies with an electron microscope JEOL 4000EX (double tilt $\pm 25^\circ$) working at 400 KV.

3. RESULTS AND DISCUSSION

3.1. SAED

3.1.1. $La_{1/3}NbO_3$. Figure 1 shows two SAED patterns corresponding to $La_{1/3}NbO_3$, one of the extremes of the solid solution. The pattern along $[010]_p$ (p refers to the basic perovskite unit cell) (Fig. 1a), presents superlattice reflections which double the c-parameter of the basic cell. This is due to the ordering of empty and occupied A-positions into alternate planes along the c-axis as it is concluded from X-ray single crystal results (18). The $[001]_p$ zone diffraction pattern (Fig. 1b), shows $(h/2\,k/2\,0)_p$ reflections which suggest a diagonal orthorhombic $\sim\sqrt{2}a_p \times \sim\sqrt{2}a_p \times \sim 2a_p$ cell. This basic cell is confirmed by HRTEM (see below and Fig. 6a). By analogy with other perovskite materials (21, 22), the reflections at $(h/2\,k/2\,0)_p$ are attributed to a tilting of the oxygen octahedra framework.

Figure 2 shows the SAED patterns along $[\bar{1}10]_p$ and $[\bar{1}14]_p$ which confirm the doubling of the c-parameter and show the presence of the $(h/2\,k/2\,l/2)_p$ reflections. Besides, there are diffuse satellite reflections at odd multiples of 1/4 $d^*(001)_p$ and at 1/6.7 $d^*(110)_p$, suggesting the existence of a modulated structure along these directions. The satellite reflections appear as two sets, symmetry related by a $\pi/2$ rotation around $[001]_p$. In fact they are not discrete spots but rods of diffuse intensity elongated along $g(\bar{1}10)_p$ (and $g(110)_p$ the second set) (Fig. 2b); this indicates that there is some disorder or faulting in the sequence of repeating units

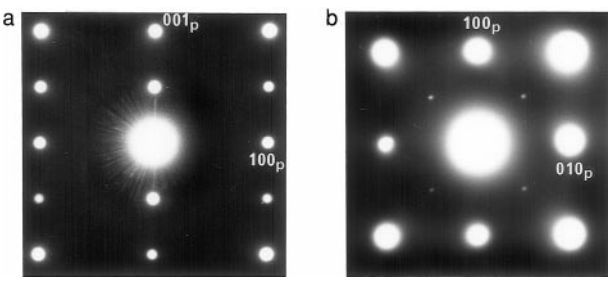

FIG. 1. SAED patterns of $La_{1/3}NbO_3$: (a) $[010]_p$ zone axis, (b) $[001]_p$ zone axis. Extra spots are present at $(0\,0\,l/2)_p$ and $(h/2\,k/2\,0)_p$.

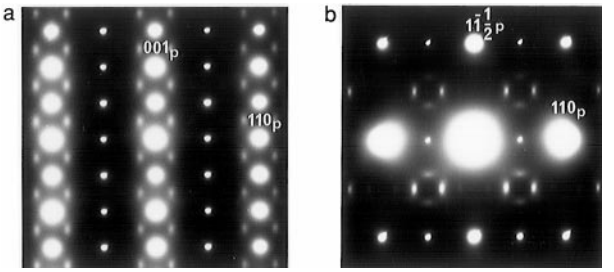

FIG. 2. SAED patterns of $La_{1/3}NbO_3$: (a) $[\bar{1}10]_p$ zone axis, (b) $[\bar{1}14]_p$ zone axis. Spots due to the modulated structure are clearly visible.

throughout these directions. Our observations on this pristine material essentially confirm the work of Labeau (18) and Labeau *et al.* (23).

3.1.2. $La_{1/3-x}Li_{3x}NbO_3$ $0 < x \leq 0.06$. Figure 3 shows representative SAED patterns of different samples of the above solid solution. The lithium-containing compounds also show a doubling of the c-lattice parameter of the basic unit cell, most probably due to the ordering of occupied and empty A-positions along alternate $(001)_p$ planes, just as the lithium-free material. Spots corresponding to the short-range modulation along two twinned directions are also observed.

On the other hand, the $(h/2\,k/2\,l/2)_p$ reflections are here replaced by a cluster of four spots in the form of a cross whose arms are parallel to $g(100)_p$ and $g(010)_p$. The splitting of the $(h/2\,k/2\,l/2)_p$ is best observed along the $[001]_p$ zone axis but can obviously be seen along other zone axes (see arrows on Fig. 3). This splitting might be due to the existence of a microdomain structure in which the system of the tilting of the octahedra around the $[110]_p$ and $[\bar{1}10]_p$ axes is twinned across intersecting $(100)_p$ and $(010)_p$ domain boundaries, as it has been observed in other A-cation deficient perovskites (24–26) as well as in the $Li_{0.5-3x}Nd_{0.5+x}TiO_3$ solid solution (11).

The combination of all these observations suggests for the niobate solid solution the reciprocal unit cell represented in Fig. 4. In the case of $x = 0$, the clusters of four spots in the form of crosses are replaced by a single spot (see Fig. 1b).

The relationship between the cubic perovskite subcell and the new supercell can be established from the electron diffraction results. As in $Th_{1/4}NbO_3$ (24), we only need to consider, in a first instance, one set of satellite reflections whose positions correspond to odd multiples of 1/4 $d^*(001)_p$ for all samples of the solid soultion and about 1/7 $d^*(110)_p$ (and about 1/7 $d^*(\bar{1}10)$ in the second set). We have observed that the incommensurability of the modulation along $g(110)_p$ does slightly vary with the lithium content of the samples, the order of the superperiodicity increasing when the amount of lithium increases (Table 1).

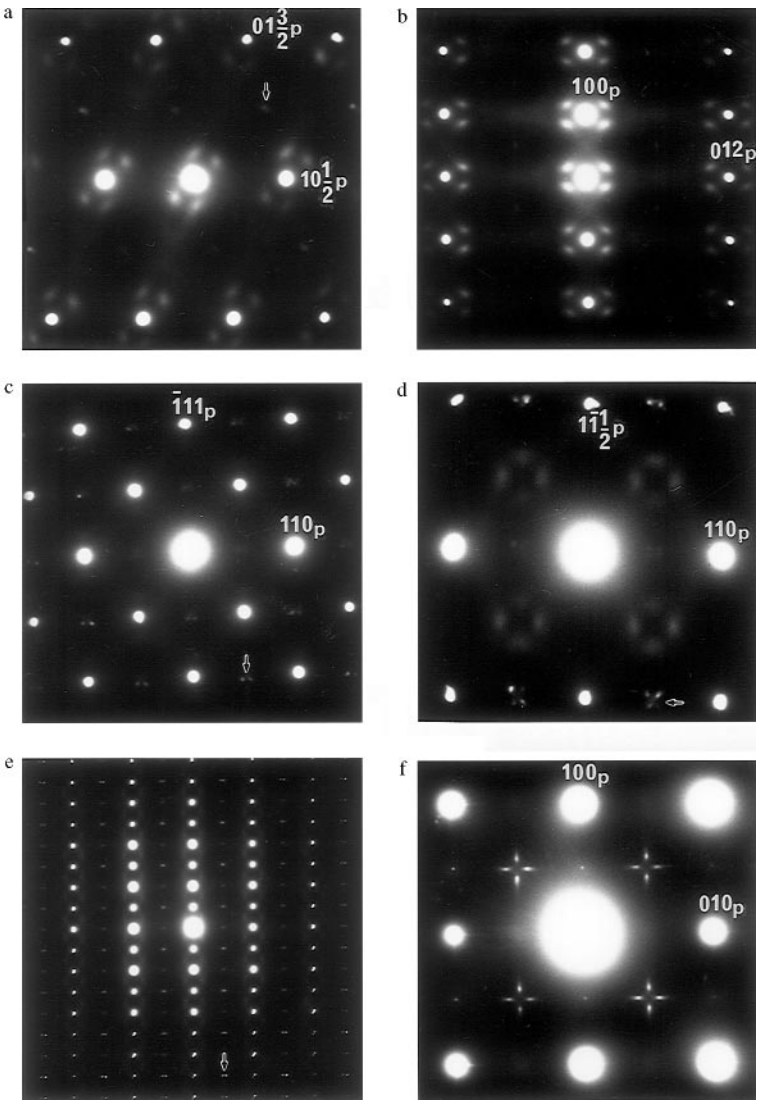

FIG. 3. SAED patterns of $La_{1/3-x}Li_{3x}NbO_3$ with $x = 0.02$: (a) $[13\bar{2}]_p$ zone axis, (b) $[0\bar{2}1]_p$ zone axis; $x = 0.04$: (c) $[\bar{1}1\bar{2}]_p$ zone axis, (d) $[\bar{1}14]_p$ zone axis and $x = 0.06$: (e) $[\bar{1}10]_p$ zone axis, (f) $[001]_p$ zone axis. Arrows signal the spliting of the spots at $(h/2\,k/2\,l/2)_p$.

Besides, we consider a single domain of octahedra tilting by replacing the "crosses" around $(h/2\,k/2\,l/2)_p$ by discrete spots at these positions. On these bases, the unit cell of these materials is related to the cubic perovskite subcell by the matrix

$$\begin{bmatrix} a \\ b \\ c \end{bmatrix} = \begin{bmatrix} 7/2 & 7/2 & 0 \\ \bar{1} & 1 & 0 \\ 0 & 0 & 4 \end{bmatrix} \begin{bmatrix} a_p \\ b_p \\ c_p \end{bmatrix}$$

which corresponds to the following axial relationship between the two unit cells: $a = 3.5(a_p + b_p) \approx 3.5\sqrt{2}a_p$; $b = -a_p + b_p \approx \sqrt{2}a_p$; $c = 4c_p \approx 4a_p$.

Taking into account the systematic absences that occur ($00l$ $l \neq 2n$), the symmetry of the new cell is most likely orthorhombic with space group $P222_1$ or monoclinic ($P2_1/m$ or $P2_1$ space group). This should be confirmed by neutron diffraction studies or single crystal X-ray data.

The incommensurate modulation can arise from atomic ordering between vacancies, lanthanum, and lithium ions within the A-positions in every other A-type plane or from small atomic displacements or both. In principle, it is possible to distinguish between the two former cases from the intensity of the satellite reflections of the diffraction patterns of thin enough crystals, in which only kinematic effects are important (27). However, proper interpretation of diffracted intensities is very complex for materials with both kinds of modulation and/or thick crystals producing dynamic scattering.

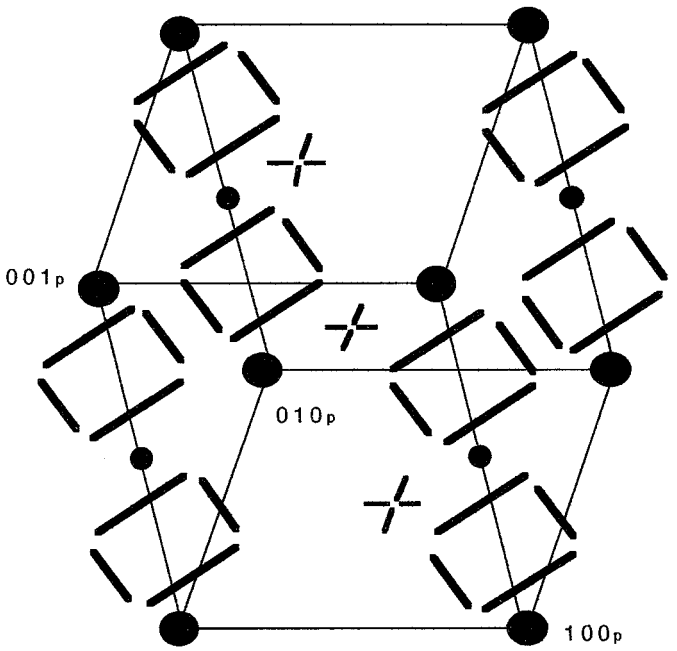

FIG. 4. Drawing of the reciprocal lattice of $La_{1/3-x}Li_{3x}NbO_3$ $0 \leq x \leq 0.06$ showing the diffraction effects as they are observed to occur in the electron diffraction patterns. When $x = 0$, the clusters of four spots in the form of crosses are substituted by single spots at $(h/2\,k/2\,l/2)_p$.

In the $La_{1/3-x}Li_{3x}NbO_3$ solid solution, the modulation is most likely due to ordering of vacancies, lanthanum, and lithium ions within the $(001)_p$ occupied planes along $g(110)_p$ (or $g(\bar{1}10)_p$ in the second kind of domains of the crystal), as it has been established in other A-cation deficient niobates (18, 24–26). The satellite reflections are elongated along $g(\bar{1}10)_p$ (and $g(110)_p$) indicating a lack of long-range correlation between $\{110\}_p$ (and $\{\bar{1}10\}_p$) planes of A-cations. The lengths of the diffuse satellites correspond to the average length or ordering which is about 20–30 Å along $g(\bar{1}10)_p$ (and $g(110)_p$). A precise determination of this length, and consequently of the real coherence length of this ordering, will require, at least, precession photographs of the $\{0\,0\,1/4\}$ planes on single crystals, which are not yet available. The fact that the satellite reflections correspond to interplanar spacing $4d(001)_p$ indicates that there is a phase shift of the modulation wave between every other occupied A-plane. Besides, a modulated displacement of the lanthanum and lithium cations along $g(110)_p$ (or $g(\bar{1}10)_p$) might also occur. This atomic displacement has been observed in related materials such as $Li_{0.5-3x}RE_{0.5+x}TiO_3$ ($x = 0.05$; $RE =$ Nd, Pr) (5), in which the Li^+-cations are strongly off-centre, and other rare earth–cation deficient perovskites (18, 24, 26). In the case of $Th_{1/4}NbO_3$ (24) and $U_{1/4}NbO_3$ (26), displacement of the niobium cations was also observed in the structure refinement on single crystals.

TABLE 1
Values of the Modulation along $g(110)_p$ (1/A d*$(110)_p$) and along $g(001)_p$ (1/B d*$(001)_p$) for $La_{1/3-x}Li_{3x}NbO_3$

x	A	B
0	6.7	4
0.02	6.8	4
0.04	7.1	4
0.06	7.3	4

The single domain model must then be completed by the incorporation of a microdomain model in which the system of the tilting of the octahedra is reflected across intersecting $(100)_p$ and $(010)_p$ domain boundaries, explaining the splitting of the $(h/2\,k/2\,l/2)_p$ reflections into four. The separation between pairs of split spots indicates superperiods of $\sim 14a_p$ along both $g(100)_p$ and $g(010)_p$ which correspond to average separations between microdomain boundaries parallel to $(100)_p$ and $(010)_p$ of $\sim 7a_p$ and $\sim 7b_p$, respectively. This separation has then practically the same magnitude as the correlation length between $\{110\}_p$ (and $\{\bar{1}10\}_p$ in other regions of the crystal) planes of ordered lanthanum, lithium, and vacancies, suggesting that the cation/vacancy ordering can be accommodated in the microdomain structure of the octhahedra tilting. It can be seen that the four reflections of the cross are elongated in the directions of the splitting and are of the same length; we can then deduce that the coherent length of the domain walls periodicity is about 60 Å along both $g(100)_p$ and $g(010)_p$, so that the cross section of the microdomains is approximately square.

3.2. HRTEM

Figure 5 shows the HRTEM images along the $[\bar{1}10]_p$ zone axis for $La_{1/3-x}Li_{3x}NbO_3$ with $x = 0$ and 0.06. The $2a_p$ periodicity along the c-axis is clearly seen. Besides, a wavy modulation along $g(110)_p$ can be observed, with an average wavelength equal to 6–7 times $d(110)_p$, consistent with the periodicity of the satellite reflections in the diffraction pattern of the corresponding zone axis (Figs. 2a and 3e). The brightness of the dots in the images also changes periodically along $g(110)_p$ and there are three, sometimes four, brighter dots in one period. This brightness variation also originates a periodicity of $4a_p$ along $g(001)_p$ in some parts of the crystal, as it is also observed in the diffraction pattern. The brightness differences of the dots seems to reflect an ordered distribution of the vacancies, lanthanum, and lithium ions along these directions.

Figure 6 shows the HRTEM images along the $[001]_p$ zone axis for $La_{1/3-x}Li_{3x}NbO_3$ compounds with $x = 0$ and 0.06. In the image of the sample with $x = 0$ (Fig. 6a), faint lattice fringes at ~ 5.5 Å corresponding to $\sqrt{2}a_p$ are observed. However, the image corresponding to a sample with

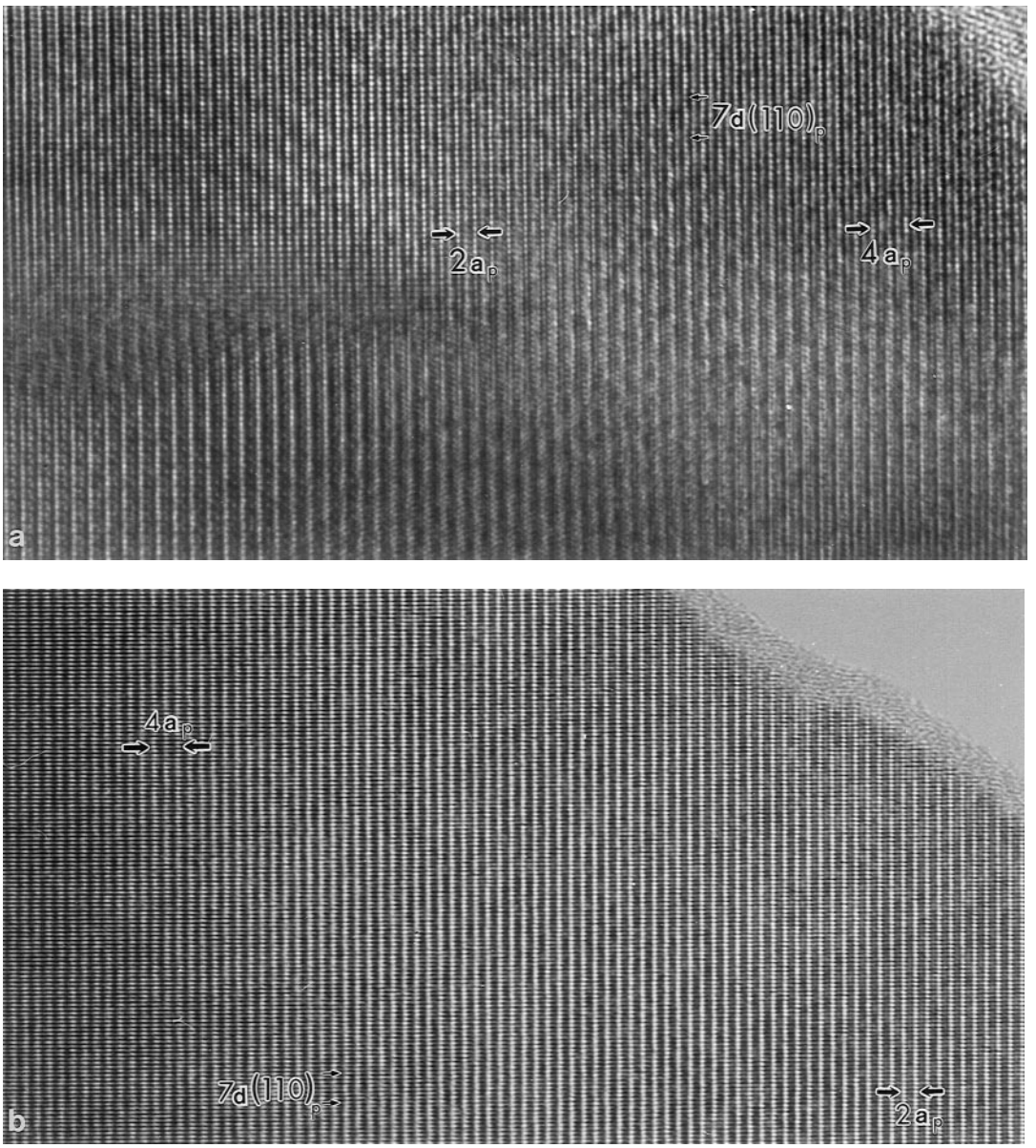

FIG. 5. HRTEM image along the $[\bar{1}10]_p$ zone axis for $La_{1/3-x}Li_{3x}NbO_3$ with $x = 0$ (a) and $x = 0.06$ (b). Continuous changes sinuously waving are obvious along $g(110)_p$.

$x = 0.06$ (and also when $x = 0.05$) (Fig. 6b) shows a patchwork-quilt array where there are regions in which ~ 7.8 Å fringes are parallel to $g(100)_p$, regions in which the ~ 7.8 Å fringes are parallel to $g(010)_p$, and areas with fringes at ~ 5.5 Å. The crystal must then be formed by randomly distributed microdomains of $a \sim \sqrt{2}a_p \times \sim \sqrt{2}a_p \times \sim 2a_p$ basic (or long-range) unit cell where in each domain the c-axis is oriented along one of the three different crystallographic directions. This explains the appearance of very weak spots at $(h/2\,0\,0)_p$ and $(0\,k/2\,0)_p$ in the diffraction pattern of the $[001]_p$ zone axis (Fig. 7c). In fact, the spots at $(0\,k/2\,0)_p$ are weaker than the ones at $(h/2\,0\,0)_p$ suggesting that in this crystal, there are more domains with the c-axis oriented along $g(100)_p$ than with the c-axis oriented along $g(010)_p$; this is indeed what can also be seen in the HRTEM image (Fig. 6b). Extra $(h/2\,0\,0)_p$ and $(0\,k/2\,0)_p$ spots do not occur in the SAED patterns of the samples with low or no lithium content (Figs. 7b and 7a, respectively), which under these conditions do not form a three dimensional microdomain structure with three different orientations of the c-axis. This kind of microdomain formation has also been observed in the $Ln_{2/3-x}Li_{3x}TiO_3$ (Ln = La, Nd) solid solutions (6, 8, 11) and seems to be correlated to the degree of orthorhombicity in materials with perovskite-related structure in a way

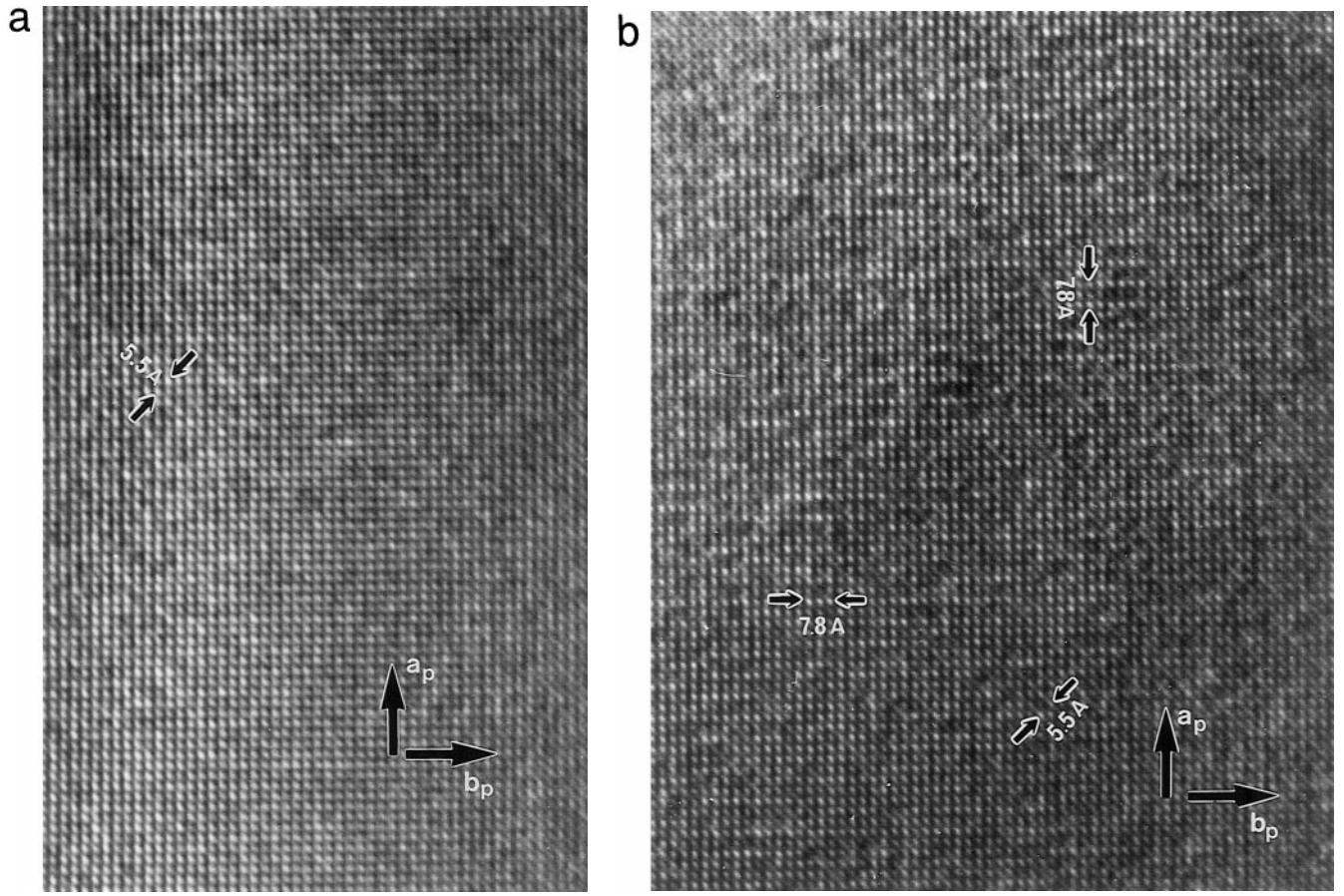

FIG. 6. HRTEM image along the $[001]_p$ zone axis for $La_{1/3-x}Li_{3x}NbO_3$ with $x = 0$ (a) and $x = 0.06$ (b). Microdomains where the c-axis ($2a_p$) is lying along each one of the three space directions are observed for the lithiated sample.

that the amount of twinning increases when the orthorhombicity of the structure decreases (28). In the $La_{1/3-x}Li_{3x}NbO_3$ compounds, the orthorhombicity of the basic structure decreases when the lithium content increases (14), which seems to explain the appearance of a microdomain structure with three different orientations of the c-axis in the samples with high lithium contents ($x = 0.05$ and 0.06).

It is worth comment that the HRTEM images of the lithium containing materials do not show any obvious evidence of the domain walls that give place to the cross-like $(h/2\,k/2\,l/2)_p$ spots. This can be attributed to the very fact that such four cross-like spots are elongated along $g(100)_p$ and $g(010)_p$, indicating that the walls are not well ordered. Obviously, the SAED pattern, covering a much larger area, gives us information about the average structure, including the domain walls.

These changes in the microstructure as a function of the lithium content are best observed in the $[001]_p$ diffraction patterns (Fig. 7) which respectively shows, for $x = 0$, no split at $(h/2\,k/2\,0)_p$ (Fig. 7a), for $0 < x \leq 0.04$, splitting of the $(h/2\,k/2\,0)_p$ reflections in the form of crosses (Fig. 7b), while for $0.05 \leq x \leq 0.06$, besides the splitting at $(h/2\,k/2\,l/2)_p$, the doubling of the perovskite cell along one direction (c_p-axis) is also three-dimensional twinned and gives an apparent doubling of both a_p and b_p axes. It is interesting to mention here that, in the case of $Th_{1/4}NbO_3$ (24, 25), the development of a microdomain texture is a function of the quenching conditions while in the case of the present samples, such ordering appears as a function of the lithium content.

4. CONCLUSIONS

Selected area electron diffraction and high resolution transmission electron microscopy studies of the $La_{1/3-x}Li_{3x}NbO_3$ ($0 \leq x \leq 0.06$) solid solution reveal that these materials have a common basic unit cell with lattice parameters $a \sim \sqrt{2}a_p$, $b \sim \sqrt{2}a_p$, $c \sim 2a_p$. Such a cell is a consequence of the ordering of vacancies within alternate $(001)_p$ planes and tilting of the NbO_6 octahedra framework. Besides, these niobate compounds, with perovskite-related structure, present a short-range modulated ordering between vacancies, lanthanum, and lithium ions within the

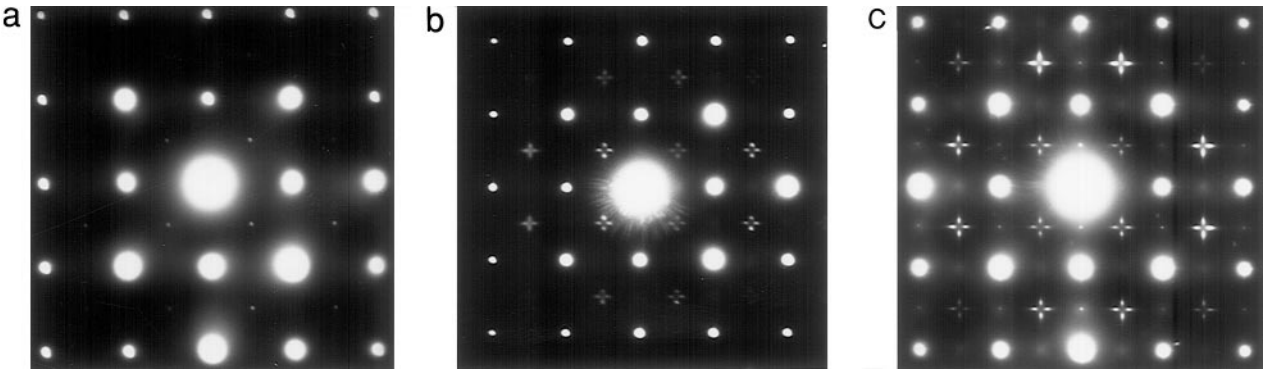

FIG. 7. SAED patterns of the $[001]_p$ zone axis reflecting the evolution of the microstructure with the composition for $La_{1/3-x}Li_{3x}NbO_3$ materials: (a) $x = 0$, with no domains; (b) $x = 0.04$, with one type of domain, and (c) $x = 0.06$, with two types of domains.

occupied $(001)_p$ planes along $g(110)_p$ (and $g(\bar{1}10)_p$ in other regions of the crystal) which lead us to propose a new unit cell with lattice parameters $a \sim 3.5\sqrt{2}a_p$, $b \sim \sqrt{2}a_p$, $c \sim 4a_p$. Moreover, the periodicity of the modulation changes with the composition of the materials, i.e., with the La/Li ratio (Table 1).

As soon as lanthanum starts to be substituted by lithium, the octahedra tilting system shows microdomains twinned across intersecting $(100)_p$ and $(010)_p$ domain boundaries so that the $(h/2\,k/2\,l/2)_p$ reflections are split into four branches in the form of a cross. The modulated ordering of the vacancies, La, and Li atoms along $g(110)_p$ (and $g(\bar{1}10)_p$) is established within these microdomains. Moreover, overimposed in this domain system, the compounds with the highest lithium content ($x = 0.05$ and 0.06) show another type of microdomain formation, as a consequence of adopting different orientations of the c-axis along one of the three crystallographic directions.

Some samples of different compositions were annealed and quenched at several temperatures or slowly cooled but microstructural changes were not observed.

ACKNOWLEDGMENTS

The authors thank CICYT (MAT95-0809, MAT-97-0697 and MAT 98-1053) and Japan Storage Battery Company for financial support. We also thank the Microscopy Centre Luis Bru from U.C.M. for the technical assistance.

REFERENCES

1. Y. Inaguma, C. Liquan, M. Itoh, T. Nakamura, T. Uchida, H. Ikuto, and M. Wakihara, *Solid State Commun.* **86,** 689 (1993).
2. Y. Inaguma, L. Chen, M. Itoh, and T. Nakamura, *Solid State Ionics* **70/71,** 196 (1994).
3. H. Kawai and J. Kuwano, *J. Electrochem. Soc.* **141,** 278 (1994).
4. A. D. Robertson, S. García-Martín, A. Coats, and A. R. West, *J. Mater. Chem.* **5**(9), 1405 (1995).
5. J. M. S. Skakle, G. C. Mather, M. Morales, R. I. Smith, and A. R. West, *J. Mater. Chem.* **5**(11), 1807 (1995).
6. A. Várez, F. García-Alvarado, E. Morán, and M. Á. Alario-Franco, *J. Solid State Chem.* **118,** 78 (1995).
7. Y. Inaguma and M. Itoh, *Solid State Ionics* **86–88,** 257 (1996).
8. J. L. Fourquet, H. Duroy, and M. P. Crosnier-López, *J. Solid State Chem.* **127,** 283 (1996).
9. O. Bohnke, C. Bohnke, and J. L. Fourquet, *Solid State Ionics* **91,** 21 (1996).
10. M. Morales and A. R. West, *Solid State Ionics* **91,** 33 (1996).
11. S. García-Martín, F. García-Alvarado, A. D. Robertson, A. R. West, and M. Á. Alario-Franco, *J. Solid State Chem.* **128,** 97 (1997).
12. J. Lee, K. S. Yoo, T. S. Kim, and H. J. Jung, *Solid State Ionics* **98,** 15 (1997).
13. Y. Harada, T. Ishigaki, H. Kawai, and J. Kuwano, *Solid State Ionics* **108,** 407 (1998).
14. S. García-Martín, J. M. Rojo, H. Tsukamoto, E. Morán, and M. Á. Alario-Franco, *Solid State Ionics* **116**(1), 11 (1999).
15. Y. Kawakami, H. Ikuta, and M. Wakihara, *J. Solid State Electrochem.* **2,** 206 (1998).
16. P. N. Iyer and A. J. Smith, *Acta Crystallogr.* **23,** 740 (1967).
17. V. K. Trunov, I. M. Averina, A. A. Evdokimov, and A. M. Frolov, *Kristallogr.* **261,** 189 (1981).
18. M. Labeau, Thesis, I.N.P. Grenoble, 1980.
19. Y. Torii, T. Sekiya, and T. Yamamoto, *Mater. Res. Bull.* **17,** 727 (1982).
20. C. C. Torardi, L. H. Brixner, and C. M. Foris, *J. Solid State Chem.* **58,** 204 (1985).
21. A. M. Glazer, *Acta Crystallogr. A* **31,** 756 (1975).
22. M. O'Keeffe and B. G. Hyde, *Acta Crystallogr. B* **33,** 3802 (1977).
23. H. Vincent, P. Wolfers, M. Labeau, M. Á. Alario-Franco, and J. C. Joubert, Int. Conference Phase Transf. Solids, Ghania (Greece), (1983), unpublished.
24. M. Á. Alario-Franco, I. E. Grey, J. C. Joubert, H. Vincent, and M. Labeau, *Acta Crystallogr. A* **38,** 177 (1982).
25. M. Labeau, I. E. Grey, J. C. Joubert, H. Vincent, and M. Á. Alario-Franco, *Acta Crystallogr. A* **38,** 753 (1982).
26. M. Labeau, Y. E. Grey, J. C. Joubert, J. Chenevas, A. Collomb, and J. C. Guitel, *Acta Crystallogr. B* **41,** 33 (1985).
27. P. R. Buseck and J. M. Cowley, *Am. Mineral.* **68,** 18 (1983).
28. A. Vegas, M. Vallet-Regi, J. González-Calbet, and M. Á. Alario-Franco, *Acta Crystallogr. B* **42,** 167 (1986).